Revista Mexicana de Astronomía y Astrofísica, **43**, 243–255 (2007)

THE NEUTRAL COUNTERPART OF AN UNCATALOGUED NEBULA AND A PROBABLE INTERSTELLAR BUBBLE AROUND WR 53 IN THE CENTAURUS REGION

M. C. Martín,[1] C. E. Cappa,[1,2] and J. C. Testori[1]

Received 2006 November 3; accepted 2007 March 2

RESUMEN

La inspección de imágenes ópticas hacia $l = 307°$ permitió encontrar una nebulosa no catalogada de $9'$ de radio, que denominamos G307.27+0.27. El análisis de la distribución de la emisión de HI reveló la presencia de una cáscara en expansión que rodea a la nebulosa. Sugerimos que la cáscara, a una distancia cinemática de 4±1 kpc, es la contraparte atómica neutra de la nebulosa. Observaciones de CO en la banda de radio y datos de la emisión en el infrarrojo lejano y medio nos permitieron detectar gas molecular y polvo interestelar asociados a las estructuras.

La presencia de una estrella O6 a una distancia compatible con la de la cáscara de HI sugiere que la estructura es una región HII o una burbuja interestelar.

Reportamos también el descubrimiento de una probable burbuja interestelar de HI relacionada a la estrella Wolf-Rayet WR 53. Sus parámetros físicos son similares a los de otras burbujas interestelares asociadas a estrellas masivas.

ABSTRACT

From the inspection of optical images at $l = 307°$ we have found an uncatalogued nebula of about $9'$ in radius, which we named G307.27+0.27. The analysis of the HI-21cm line emission distribution revealed an expanding HI shell that encircles the optical emission region. The shell, placed at a kinematical distance of 4±1 kpc, is suggested to be the HI counterpart of the optical nebula. CO observations at radio wavelengths, and far and mid IR data, allowed us to detect molecular gas and interstellar dust associated with the structures.

The presence of an O6 star at a spectrophotometric distance compatible with that of the shell supports a stellar wind/HII region origin for the whole structure.

We also report a probable HI interstellar bubble related to the Wolf-Rayet star WR 53. Its physical parameters are similar to the parameters of other HI bubbles around massive stars.

Key Words: **ISM: BUBBLES — ISM: HII REGIONS — STARS: WOLF-RAYET**

1. INTRODUCTION

Massive stars interact with the surrounding interstellar gas through different processes, strongly modifying the distribution of the interstellar matter in the Galaxy. Their UV photon flux ionizes the neutral atomic gas forming HII regions. Along with stellar winds and supernova explosions, this mechanism gives origin to cavities and shells that can be detected in a large range of wavelengths, from the optical to the radio range. The HI 21 cm line emission distribution has proved to be a very useful tool to analyze the structure, kinematics and energetics of these features, which appear as central cavities surrounded by expanding neutral envelopes (Dubner 2002; Deharveng et al. 2003; Cappa et al. 2003).

In this paper we report on the identification of an optical nebula of about $9'$ in size, centered at $(l,b) = (307°16', +0°16')$ as well as an HI shell, which is suggested to be the neutral gas counterpart of the ionized nebula; and of a probable HI interstellar bubble associated with the Wolf-Rayet star HD 117297

[1]Instituto Argentino de Radioastronomía, CONICET, Argentina.

[2]Facultad de Ciencias Astronómicas y Geofísicas, Universidad Nacional de La Plata, Argentina.

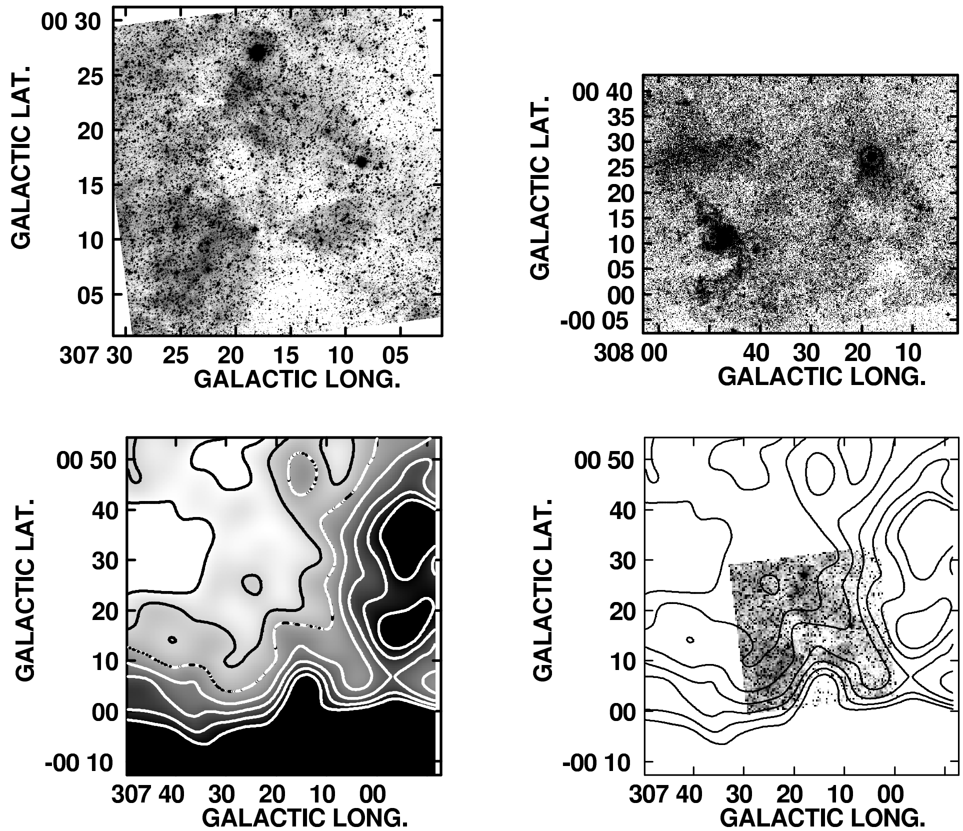

Fig. 1. *Top left panel*: Hα image of G307.27+0.27. *Top right panel*: DSS R image of the nebula (in the right section of the image), including RCW 78 (in the left section). *Bottom left panel*: High-resolution visual absorption map in grayscale from 0.4 to 1.0 mag and contour lines from 0.4 to 1.0 mag in steps of 0.1 mag. *Bottom right panel*: Overlay of the visual absorption image in contour lines and the Hα image.

($\equiv$ WR 53, van der Hucht 2001). In the next sections we analyze these structures and their counterparts at different frequencies, and investigate their origin.

The analyzed region corresponds to an area of about 1° in size centered at $(l, b) = (307°20', +0°25')$. It is encompassed between two large areas with plenty of HII regions, radio continuum sources, dust clouds and molecular gas. The "305-complex", located between $l=$ 305°and 306°(as defined by Georgelin et al. 1988), is known as a massive star forming region associated with WR 48a and the open clusters Danks 1 and 2 (Clark & Porter 2004). The HII regions RCW 78 (related to WR 55), RCW 79, RCW 80, G307.57-0.62, G307.62-0.32 and G309.06+0.19 (Caswell & Haynes 1987; Kuchar & Clark 1997) are located at $b > 307.5°$.

2. DATA BASES

To accomplish this study we used HI, radio continuum and molecular data retrieved from different sources.

The HI 21 cm line data analyzed in this paper belong to the Southern Galactic Plane Survey (SGPS), obtained using the Australia Telescope Compact Array (ATCA) and the Parkes Radiotelescope, which provided the short spacing information. The neutral gas data were obtained with a synthesized beam of $2'.2 \times 2'.2$, a velocity resolution of 0.82 km s^{-1} and an rms noise of 1.5 K. The velocity coverage of the HI data spans the range -145 to $+184$ km s^{-1}. A complete description of the survey can be found in McClure-Griffiths et al. (2005).

Radio continuum data at 4.85 GHz are available from the Parkes-MIT-NRAO (PMN) Southern Radio Survey (Condon, Griffith, & Wright 1993), and at 2.4 GHz from Duncan et al. (1995). The angular resolution and rms noises are 5′ and 7.7 mJy beam^{-1} for the 4.85 GHz survey, and $10'.4$ and 12 mJy beam^{-1} for the 2.4 GHz survey, respectively.

The analysis of the molecular gas distribution was based on the CO survey by Dame, Hartmann, & Thaddeus (2001). The angular resolution of these

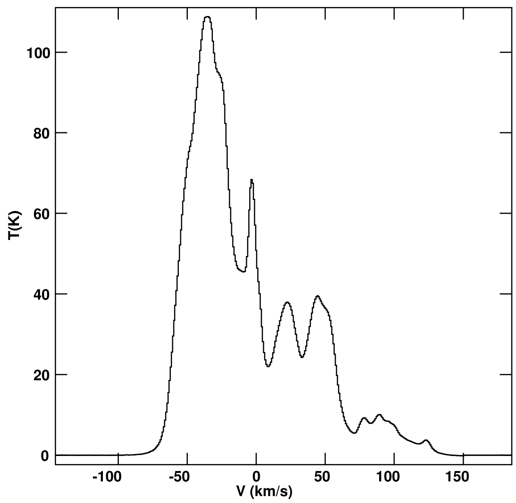

Fig. 2. Average HI spectrum within the analyzed region.

data is 8.′8. The velocity coverage and the velocity resolution are −160 to +160 km s^{-1} and 1.3 km s^{-1}, respectively. The rms noise level is 0.2 K.

The dust distribution in the region was studied using the high-resolution (HIRES) IRAS data obtained through *IPAC* [3]. The IR data in the *IRAS* bands at 60 and 100 μm have angular resolutions of 1.′2 and 2.′0, respectively. We have also inspected the mid IR emission distribution using the images of Midcourse Space Experiment (MSX) through IPAC, which have an angular resolution of 18.4′′.

Optical images were obtained from the AAO/UKST SuperCOSMOS H-alpha Survey (SHS) by Parker et al. (2005), and from the Digitized Sky Surveys ESO/ST (DSS R).

3. G307.27+0.27 AND ITS NEUTRAL GAS COUNTERPART

3.1. *The optical nebula*

The upper left panel of Figure 1 shows the Hα image of a region of 30′ in size centered at *(l,b)* ≅ (307°16′, +0°16′). The image reveals the presence of patchy optical emission delineating an almost complete shell-like nebula of about 9′ radius. The central region lacks optical emission. The nebula is barely visible in the Hα photograph by Georgelin et al. (1988). We named this uncatalogued nebula G307.27+0.27. The upper right panel displays the DSS R image of a larger field of view. G307.27+0.27 is clearly detected in this image, as well as RCW 78.

[3] *IPAC*=Infrared Processing and Analysis Center, is funded by NASA as part of the IRAS extended mission under contract to Jet Propulsion Laboratory (JPL) and California Institute of Technology (Caltech).

The distribution of the interstellar extinction toward G307.27+0.27, as derived from star counts (Dobashi et al. 2005), is shown in the bottom left panel of Figure 1 (in grayscale and contours), while the bottom right panel displays an overlay of the same contours and the optical image. A region of slightly higher absorption coincides with the center of the optical structure, where optical emission is lacking, suggesting that the shell-like appearance of the optical feature may originate by the presence of foreground interstellar dust.

3.2. *HI emission distribution*

With the aim of investigating the distribution of the neutral atomic hydrogen, we analyzed the HI 21 cm line emission distribution in the environs of the nebula using *(l,b)* images at constant velocity. For presentation purposes, a constant background equal to the mean value of each channel map was subtracted from every map. Figure 2 shows the subtracted spectrum, which corresponds to the average HI spectrum within the analyzed area. HI is detected within the velocity interval −70 to +125 km s^{-1}. According to the circular galactic rotation model of Brand & Blitz (1993), gas with velocities ≤−15 km s^{-1} is placed at distances $d \geq$ 1 kpc and belongs to the Carina and Scutum-Crux spiral arms (Caswell & Haynes 1987), while velocities of ≈0 km s^{-1} correspond to gas in the Local spiral arm. Gas with positive velocities at +22 and +50 km s^{-1} should be located outside the solar circle, at about 12 and 15 kpc, respectively.

Figure 3 displays a series of images showing the neutral hydrogen emission distribution within the velocity range −67.2 to +7.0 km s^{-1}. Each individual image is the result of integrating the HI emission within a velocity interval of 4.1 km s^{-1}. The cross in the figures indicates the position and size of G307.27+0.27.

The figure reveals the presence of a number of low HI emission regions at different velocities. Most of them are present within a velocity interval of a few km s^{-1}, compatible with the velocity dispersion of neutral gas in the interstellar medium. The HI cavity and shell near *(l,b)*=(307°18′, +0°18′), close to the center of G307.27+0.27, are present within the velocity range from −54.8 to −26.1 km s^{-1}. The cavity appears almost completely encircled by regions of enhanced emission. The systemic velocity of the structure, defined as the velocity at which the cavity and the envelope present their largest dimensions, is $v_{\rm sys}$=−42 km s^{-1}.

The radial velocity of this structure is in excellent agreement with the radial velocities of the "305°

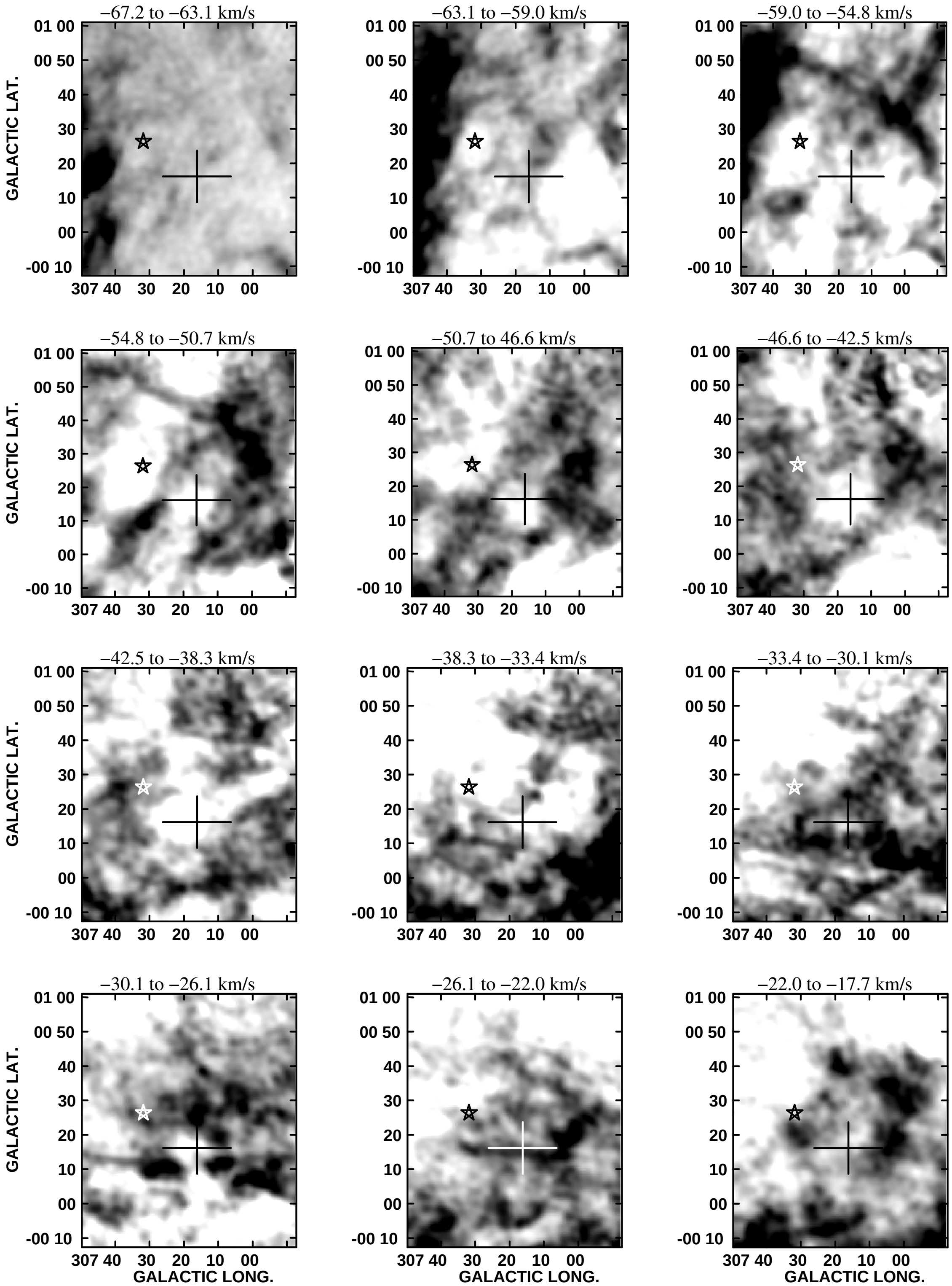

Fig. 3. HI emission distribution within the velocity interval from −67 to +7 km s^{-1} in steps of 4.1 km s^{-1}. The velocity interval of each map is indicated in the upper part of the images. The grayscale is from −10 to 20 K. The position and size of G307.27+0.27 are indicated by the cross. The star symbol marks the location of WR 53.

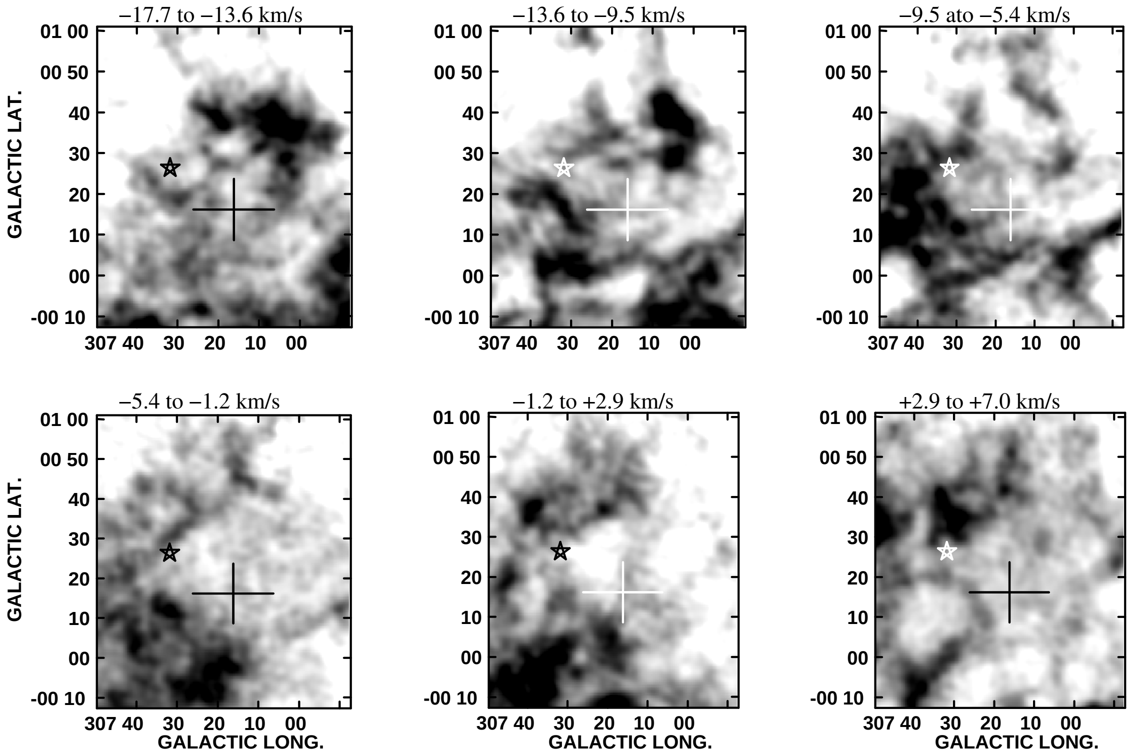

Fig. 3. Continued.

complex" and most of the HII regions at $l \geq 307°20'$ (from -52 to -37 km s^{-1}, Georgelin et al. 1988).

The top panel of Figure 4 shows the HI brightness temperature integrated within the velocity range -46.6 km s^{-1} to -38.3 km s^{-1}, where the cavity and shell are better defined and have their larger dimensions. No average HI emission was subtracted from this image. The HI structure, named GSH 307.3+0.3–42, is approximately spherical in shape with a diameter of $\cong 36'$. The thickness of the shell is small toward *(l,b)* $\cong$ (307°22′,+0°27′), where the cavity connects to another void centered near *(l,b)* $\cong$ (307°30′,+0°50′).

The analytical fit to the circular galactic rotation model (Brand & Blitz 1993) predicts that gas at ≈ -42 km s^{-1} is located at kinematical distances of $\approx 4.0\pm1.0$ kpc or $\approx 6.4\pm1.0$ kpc. This distance range corresponds to material in the Scutum-Crux spiral arm. The uncertainty in the near and far kinematical distances was estimated adopting a velocity dispersion of 6 km s^{-1}.

The central and bottom panels of Figure 4 show a superposition of the optical and the HI structures. They reveal that the ionized feature coincides with the HI cavity. The relatively faint shell-like optical structure appears encircled by the neutral shell. The morphological correspondence between the optical emission and the borders of the HI void strongly suggests that both features are related.

3.3. *Counterparts of G307.27+0.27 and GSH 307.3+0.3–42 at different wavelengths*

3.3.1. *Radio continuum emission*

Radio continuum data of this region are available at 4.85 GHz from the Parkes-MIT-NRAO (PMN) Southern Radio Survey (Condon et al. 1993), and at 2.4 GHz from Duncan et al. (1995).

The inspection of the radio continuum images at these frequencies shows no radio emission related to G307.27+0.27. The lack of detectable radio continuum emission is compatible with the low Hα emission. Following the expression (11) by Dickinson, Davies, & Davies (2003), we can estimate the expected radio continuum emission from the intensity of the Hα line. For an electron temperature $T_e = 10^4$ K, a frequency ν=4.85 GHz, and the ratio between the accurate formalism for the free-free optical depth given by Oster (1961) and adopting a $\simeq 1$, that expression gives T_b^{ff}=351.9 $I_{H\alpha}$, where T_b^{ff} is the brightness temperature from free-free emission.

The mean value of the Hα emission was obtained from the SuperCOSMOS Hα image displayed in Fig-

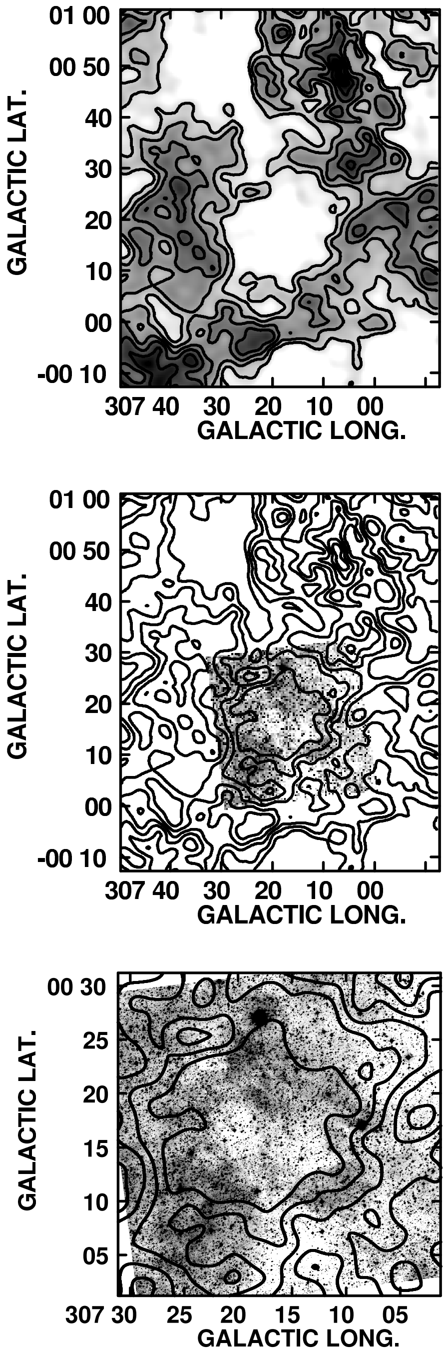

Fig. 4. *Top panel*: H I column density distribution toward GSH 307.3+0.3–42, within the velocity range -46.6 km s^{-1} to -38.3 km s^{-1}. The grayscale is from 85 K to 115 K. Contour lines correspond to 90 K to 125 K in steps of 5 K. *Central panel*: Overlay of the total H I distribution (contour lines) and the Hα image. *Bottom panel*: Overlay of the H I distribution (contour lines) and the Hα image in a region of $30'$ in size centered on G307.27+0.3.

ure 1 (top left panel). We subtracted the optical continuum emission using the SR image available at the SHS web page, as indicated by Parker et al. (2005), and averaged the Hα emission within the region showing optical emission. To convert from SuperCOSMOS units (intensity counts) to Rayleighs we applied the factor 13.8 counts/pixel/R, given by Pierce (2005). We obtained a mean value $I_{H\alpha}$=280 R over the region. The expected T_b^{ff} is then 0.025 mK.

The rms noise of the radio continuum image at 4.85 GHz is 7.7 mJy, which corresponds approximately to 4 mK. This value is larger than the expected free-free brightness temperature.

Also, the low emission measure of the ionized region, along with the poor angular resolution of the radio observations in comparison with the small size of the cavity, may contribute to leave the structure undetected.

3.3.2. *CO emission*

The top panel of Figure 5 shows the CO emission integrated over the velocity range -46.8 to -37.7 km s^{-1}, while the bottom panel displays an overlay of this image and the H I emission distribution. Although the relatively low angular resolution of the CO data precludes a detailed morphological comparison, molecular emission probably associated with the H I shell is clearly noticed. The images reveal the coincidence between regions of low molecular emission and the H I void corresponding to GSH 307.3+0.3–42 as well as the one centered at *(l,b)* $\cong$ (307°30′,+0°50′).

The brightest CO emission region at *(l,b)* $\cong$ (306°53′,+0°36′) appears projected well outside the borders of the optical nebulosity and the neutral shell. The CO emission extends towards *(l,b)* $\cong$ (307°10′,+0°05′) and *(l,b)* $\cong$ (307°20′,+0°25′). These molecular emission regions may be linked to G307.27+0.27 and GSH 307.3+0.3–42.

Other bright CO emission regions at *(l,b)* $\cong$ (307°50′,+0°6′) and *(l,b)* $\cong$ (307°36′,−0°12′) are probably related to the H II regions RCW 78 [*(l,b)* = (307°51′,+0°13′)] and G307.620-0.320 (Caswell & Haynes 1987), respectively.

3.3.3. *Far IR emission*

The IR emission at 100μm is shown in the top panel of Figure 6 in grayscale and contour lines, while the central panel displays an overlay of the IR contours and the Hα image. This figure reveals the presence of an interstellar dust patch projected onto the center of the optical feature. The IR lane running from *(l,b)* $\cong$ (307°10′,+0°) to $\cong$ (307°20′,+0°15′) is

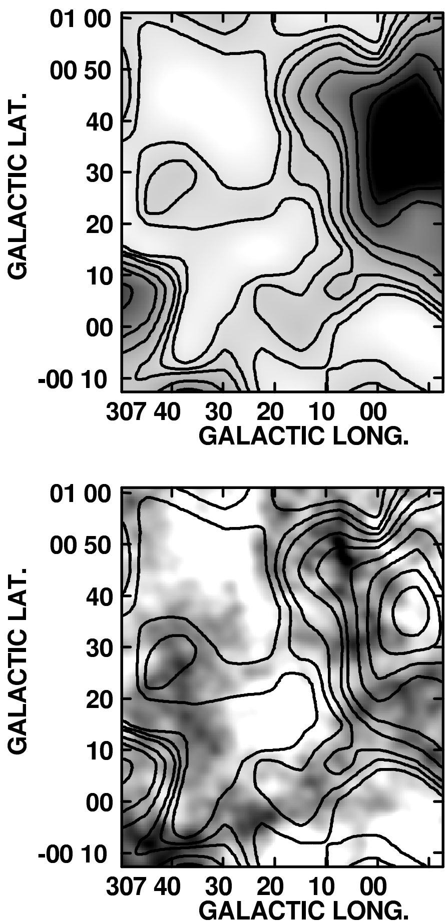

Fig. 5. *Top panel*: CO brightness temperature distribution within the velocity range of -46.8 km s^{-1} and -37.7 km s^{-1}. The grayscale corresponds to 0.2 to 2.0 K, and the contour lines are from 0.4 K to 0.6 K in steps of 0.1 K and from 1.0 K to 2.6 K in steps of 0.4 K. *Bottom panel*: Overlay of the same CO contour lines and the HI emission distribution (grayscale) within the velocity range -46.6 km s^{-1} to -38.3 km s^{-1}.

projected onto the region lacking optical emission towards the center of G307.27+0.27.

The search for molecular emission associated with this IR lane revealed that CO emission at v=-28 km s^{-1} (at $\approx$ 2 kpc according to circular galactic rotation models) coincides with the IR emission (see the bottom panel of Figure 6). The interstellar dust lane is then possibly linked to this molecular cloud at $\approx$ 2 kpc, and may be responsible for the absorption towards the center of the optical feature. This fact reinforces the suggestion pointed out in §3.1, concerning the posibility that the shell-like appearance of the optical feature originates by the presence of foreground interstellar dust.

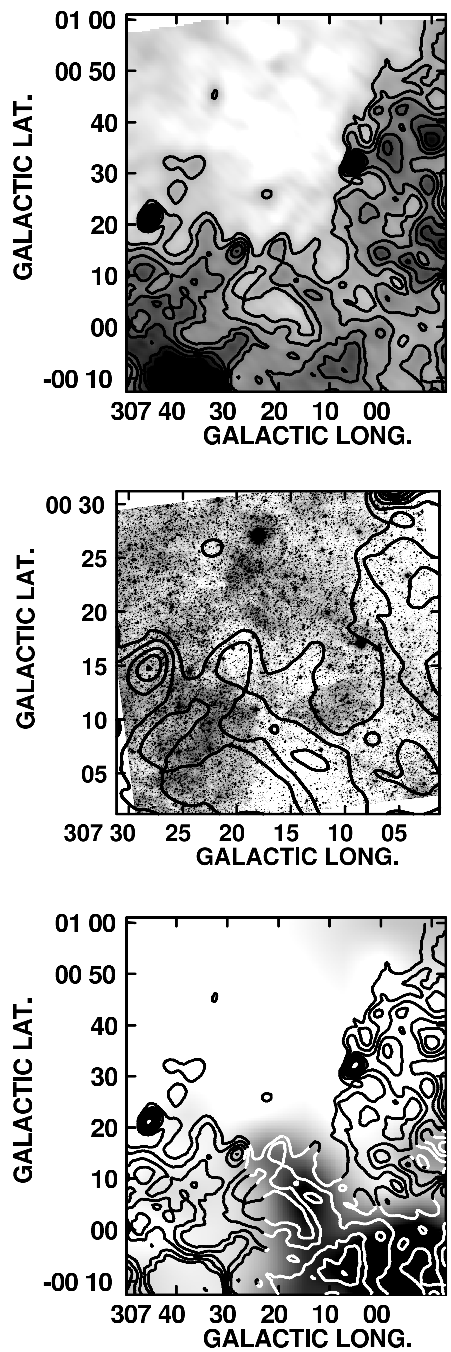

Fig. 6. *Top panel:* Far IR emission distribution at 100μm. The grayscale is from 0 to 400 MJy ster^{-1} and the contour lines are 110, and from 150 to 400 MJy ster^{-1} in steps of 50 MJy ster^{-1}. *Central panel:* Overlay of the far IR emission (contour lines) and the optical Hα image of a region of 30$'$ in size centered on G307.27+0.27. *Bottom panel:* Overlay of the far IR emission (contour lines) and the CO brightness temperature at -28 km s^{-1} (grayscale).

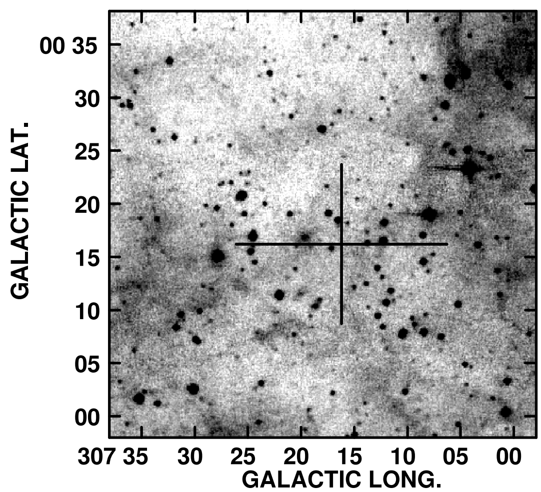

Fig. 7. MSX A-Band emission distribution. The position of the cross marks the center of G307.27+0.27. Its size indicates to the extension of the optical nebula.

3.3.4. *Near IR emission*

Figure 7 shows the IR emission in the MSX A-Band (8μm). The image reveals the presence of a weak arc-like emission region near *(l,b)*=(307°17′, +0°27′), of about 20′ in size, located just outside the ionized region. This arc appears projected at the interface between the ionized nebula and the neutral gas at *(l,b)*=(307°20′, +0°30′). Other patches of IR emission are detected bordering G307.27+0.27, at $b \leq +0°15'$. Weak emission is also coincident with the central region of G307.27+0.27. No emission was detected in the other three bands.

Emission in the A-band is commonly attributed to polycyclic aromatic hydrocarbons (PAHs, Leger & Puget 1984). PAHs are destroyed by the UV radiation in HII regions, but can survive in the outkirts of ionized regions (Cesarsky et al. 1996).

We believe that the MSX 8μm image gives additional support to the presence of an HII region.

3.4. *Discussion: the possible origin of the structures*

3.4.1. *Related stars*

With the aim of investigating the origin of the structure we searched for massive stars toward *l*=307°, which may have originated G307.27+0.27 and GSH 307.3+0.3–42 through UV photons or stellar winds. We confined our search to a region of 20′ in radius centered at the position of G307.27+0.27. Table 1 lists the O and WR stars within this region.

The open cluster Basel 18, of about 6′ in size, is projected onto the border of the optical nebula at *(l,b)*=(307°11′, +0°12′). Distance estimates to Basel 18 are 1.5 kpc (Subramaniam et al. 1995) and 2.23 kpc (Dias et al. 2002). Bearing in mind the kinematical distance derived for the HI shell, we believe that the stellar cluster is in front of the structure.

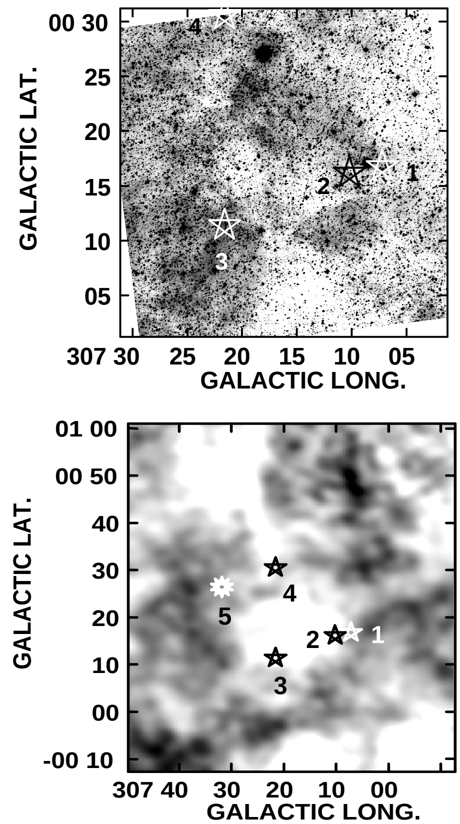

Fig. 8. O-type and WR stars projected onto the Hα image (top panel) and the HI emission distribution (bottom panel). The five-point stars indicate the positions of the O-type stars, while the ten-point star marks the location of WR 53.

The positions of the O and WR stars are plotted in Figure 8 superposed onto the optical and HI images. The figures show that S 214, S 221 and S 240 are projected near the border of G307.27+0.27. The location of CD–61°3799 and WR 53, outside the borders of the optical structure do not favor their association with the optical feature.

Distances to O-type stars were estimated taking into account absolute magnitudes and intrinsic colors from Vacca, Garmany, & Shull (1996). The O-type stars S 214, S 221, and S 240 were extracted from the list of faint O-B stars in Centaurus by McGruder (1975). The magnitudes and colors measured by McGruder have large errors, quoted in the table with a colon ":" and a double colon "::". This author

TABLE 1

O-B3 AND WR STARS TOWARDS THE ANALYZED REGION

#	Star	*(l,b)*	Sp.T.	*V* mag	*(B-V)* mag	*d* kpc
1	S 214[a]	307°07′ 30.6″ +0°16′ 30.1″	O6V	13.69	3.49::	0.3±0.1
			(O6I)	13.69	3.49::	0.5±0.3
			(O6III)	13.69	3.49::	0.4±0.2
2	S 221[a]	307°10′ 05.7″ +0°16′ 07.0″	O6V	12.98::	1.98:	1.8±0.9?
			(O6I)	12.98::	1.98:	3.0±1.7
			(O6III)	12.98::	1.98:	2.5±1.4
3	S 240[a]	307°21′ 34.1″ +0°11′ 32.1″	O6V	14.43	2.66:	1.4±0.6?
			(O6I)	14.43	2.66:	2.2±1.3
			(O6III)	14.43	2.66:	1.8±1.0
4	CD-61°3799[b]	307°21′46.9″ +0°30′24.4″	O...			
5	HD 117297=WR 53[c]	307°31′ 55.6″ +0°26′ 16.3″				1.9−5.3[d]

[a]McGruder (1975).

[b]Simbad Data Base (Centre de Données Astronomiques de Strasbourg).

[c]van der Hucht (2001).

[d]Conti & Vacca (1990); Smith, Shara, & Moffat (1990); van der Hucht (2001).

suggested that the three stars may be of luminosity class I or III, instead of V. Consequently, we included in the table the distances to these stars corresponding to luminosity classes I, III, and V. Uncertainties in the distance estimates were obtained assuming a moderate error $\Delta(B-V) = 0^{\mathrm{m}}.4$.

The derived distance estimates indicate that S 214 and S 240 are closer to the Sun than the HI structure. The distance to S 221 is compatible with the near kinematical distance to GSH 307.3+0.3–42. We suggest as a working hypothesis that this O-type star may have originated the optical and neutral features. S 221 is projected onto the optical emission region, close to the high density section of the HI shell.

The O6 star S 221 is then the only detected source of UV photons and/or stellar winds capable of creating the stucture. We adopt the near kinematical distance for GSH 307.3+0.3–42 (4.0±1.0 kpc) and, consequently, for G307.27+0.27.

3.4.2. *Testing the hypothesis*

Assuming that G307.27+0.27 is a typical HII region, we can derive upper limits for the electron density n_e and the ionized mass M_i from the rms flux density at 4.85 GHz. Adopting $R = 9'$ as the radius of the HII region, we estimate an upper limit for the flux density $S_{4.85GHz}$=300 mJy. The physical parameters of the HII region can be obtained using the expressions by Mezger & Henderson (1967) for a spherical ionized region of constant density. Adopting an electron temperature of 10^4 K and a volume filling factor $f = 1.0$, we derive $n_e \cong 2$ cm^{-3} and $M_i \cong 900\ M_\odot$. We have assumed a 10% He abundance and that He is singly ionized.

From the observed radius R of the cavity and the electron density we find that the UV stellar photon flux required to ionize the gas is $N_L \cong 2 \times 10^{47}$ s^{-1}. This value corresponds to O-type stars and is more than an order of magnitude lower than the UV photon flux emitted by an O6 star ($N_L > 10^{49}$ s^{-1}) (Martins, Schaerer, & Hillier 2005), implying that the star is capable of creating the HII region. Thus, a small number of the stellar UV photons are used to ionize the gas in the inner region of GSH 307.3+0.3–42.

The main physical parameters of the neutral gas structure probably associated with the O-type star S 221 are summarized in Table 2. The velocity interval corresponds to the range where the HI structure can be identified, with v_1 and v_2 being the lowest and highest velocities at which the HI feature is detected. The systemic velocity is the velocity at which the structure presents its largest dimension. The expansion velocity was estimated as $v_{\rm exp}$=$(v_1 - v_2)/2$

TABLE 2

MAIN PARAMETERS OF GSH 307.3+0.3–42 AND THE HI BUBBLE AROUND WR 53

	GSH 307.3+0.3–42	HI bubble around WR 53
(l,b) Center	307°18′,+0°18′	307°34′,+0°30′
Velocity interval (v_1,v_2)	−55,−26 km s^{-1}	−61,−50 km s^{-1}
Systemic velocity (v_{sys})	−42 km s^{-1}	−55 km s^{-1}
Expansion velocity (v_{exp})	15 km s^{-1}	8 km s^{-1}
Kinematical distance	4.0±1.0 kpc	5.0±1.0 kpc
Radius of the HI cavity	11′ or 12.7±3.2 pc	11.′6 or 16.9±3.4 pc
Radius of the HI structure	18′ or 20.8±5.2 pc	18′or 26.2±5.2 pc
Swept-up atomic mass	950±470 $M_\odot$	3400±1400 $M_\odot$
Ionized mass (M_i)	900±450 $M_\odot$	—
Kinetic energy (E_k)	4×10^{48} erg	2×10^{48} erg
Dynamical age (t_d)	8×10^5 yr	2×10^6 yr

+1.6 km s^{-1}. The extra 1.6 km s^{-1} allow for the presence of HI in the caps, which in this case are not detected. The radius of the HI cavity was estimated considering the contour line of 90 K, and the radius of the HI structure was obtained from the position of the maxima in the envelope. The swept-up neutral mass is the mass excess in the envelope. Errors in the parameters correspond to the uncertainty in the adopted distance.

The kinetic energy of the interstellar structure E_k=$M v_{\rm exp}{}^2/2$ was derived from the expansion velocity, taking into account the sum of the neutral and ionized mass. The original ambient density obtained by distributing the neutral and ionized masses within the volume of a sphere of ≈ 27 pc radius is n_o=2 cm^{-3}.

For an interstellar bubble, the dynamical age can be estimated as t_d=0.55 × 10^6 $R/v_{\rm exp}$ yr (McCray 1983), where R is the radius of the HI structure, $v_{\rm exp}$ is the expansion velocity and the constant represents a mean value between the energy and the momentum conserving cases.

The ratio between the kinetic energy (E_k) and the mechanical energy of the stellar wind (E_w) is E_k/E_w=ϵ, where ϵ is the energy conversion efficiency. Adopting conservative values for the mass loss rate and terminal velocity of an O6 star ($\dot{M}$=1 × 10^{-6} $M_\odot$/yr and V_w=2000 km s^{-1}, respectively) and that the wind is blowing at least during 3 × 10^6 yr, the mechanical luminosity L_w (=$\dot{M}$ $V_w{}^2/2$)=1.3 × 10^{36} erg s^{-1}, and E_w (=L_w t_d)=1.2 × 10^{50} erg. Taking into account the kinetic energy listed in Table 2, ϵ ≅ 0.035. Similar results were found for stellar wind HI interstellar bubbles around massive stars, implying that the mechanical energy released by the O6 star into the interstellar medium would be enough to create an interstellar bubble. The characteristics and physical parameters of GSH 307.3+0.3–42 are similar to those of HI interstellar bubbles around both WR and O-type stars (e.g. Cappa et al. 2003).

Very probably, most of the stellar UV photons and the stellar wind mechanical energy escape from GSH 307.3+0.3–42 through the patchy envelope, as suggested by Cooper et al. (2004) for the wind-blown bubble Sh2-308, and may contribute to energize the HI structure centered at *(l,b)*=(307°30′, +0°50′).

Note that the dynamical age is lower than the main sequence lifetime of a massive star. Uncertainties in the expansion velocities and in the expansion law of the bubble may be responsible for the derived low value.

An off-center stellar position within a quite spherical bubble, as is the case for GSH307.3+0.3–42, can be explained by a relatively low stellar motion and/or by the presence of a density gradient in the ISM where the interstellar bubble is evolving. The first case was analyzed by Weaver et al. (1977),assuming that the star is originally close to the center of the structure. The effect of a large stellar motion on an interstellar bubble is to distort the structure in the direction of the stellar motion. Using expresion (64) by Weaver et al. (1977), we find that for $t \leq 3 \times 10^6$ yr, the interstellar bubble will not be distorted if the stellar velocity is ≤ 13 km s^{-1}. This is a low tangential stellar velocity corresponding to an undectectable proper motion.

The second case was studied by Dyson (1977). In a region with a density gradient, the section of the shell moving towards higher density regions decelerates rapidly, while the section moving towards lower density regions decelerates more slowly. S 221 is projected close to one of the higher density regions, as the CO emission distributions shows (see Figure 5), making this hipothesis probable.

A supernova explosion can also create a similar structure. However, G307.27+0.27 does not have the typical filamentary appearance of a SN remnant in the optical range. Besides, the presence of the O6 star at a distance compatible with that of GSH 307.3+0.3–42 favors a stellar wind/HII region interpretation.

4. AN HI INTERSTELLAR BUBBLE AROUND WR 53?

The Wolf-Rayet star WR 53 (= HD 117297, WC8d, van der Hucht 2001) is located at *(l,b)* = (307°31.′8, +0°26.′4), coincident with a region of diffuse HII emission (Marston, Chu, & Garcia-Segura 1994). The star appears projected onto the HI shell GSH 307.3+0.3–42. Distance estimates to this star are in the range 1.9-5.3 kpc (Conti & Vacca 1990, Smith et al. 1990, van der Hucht 2001).

The analysis of the HI emission distribution at different velocities towards WR 53 (Figure 3) shows the presence of a low emission region centered near the position of the WR star, spanning the velocity interval −61 to −50 km s^{-1}. The integrated HI emission is displayed in Figure 9. The cavity is surrounded by regions of enhanced emission which are better identified towards higher galactic latitudes and higher galactic longitudes. Towards higher galactic longitudes, the steep HI gradient suggests the presence of piled-up neutral gas. The structure is elongated, of 45′×28′ in size. The systemic velocity of this structure is −55 km s^{-1}.

The circular galactic rotation model by Brand & Blitz (1993) predicts that gas at this velocity is placed at a kinematical distance of 5±1 kpc. This value is compatible with the spectrophotometric distance to the WR star.

Patchy CO emission is detected towards the region of WR 53 within the velocity range −61 to −50 km s^{-1}. Although the CO emission coincides with regions showing HI emission, the association of the molecular gas with the HI structure is doubtful. No clear dust emission related to this structure is detected in the IRAS images. The image corresponding to the MSX band-A shows patchy emission projected onto both the cavity and the surrounding shell. However, its association with the HI structure is not clear.

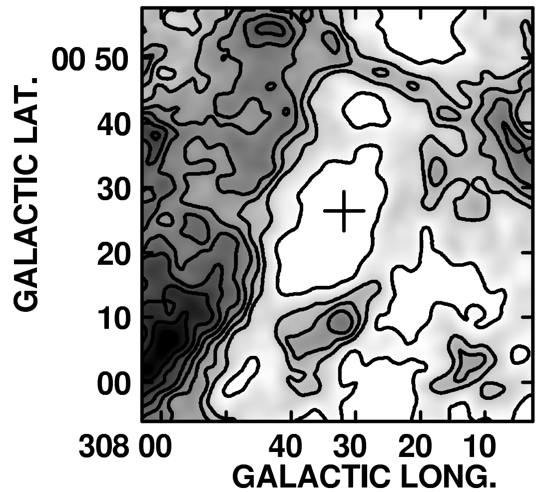

Fig. 9. HI emission distribution towards WR 53, within the velocity range −61 km s^{-1} to −50 km s^{-1}. The grayscale is from 45 to 90 K. Contour lines correspond to 45 to 90 K in steps of 5 K.

The main physical parameters of the HI structure around WR 53 are summarized in Table 2. The radius of the HI hole was estimated taking into account the contour line corresponding to 45 K.

We can estimate the stellar wind energy E_w necessary to blow the HI bubble around WR 53. Adopting $\epsilon = 0.03$ (a value obtained from the study of a large number of HI interstellar bubbles, see Cappa et al. 2003), and the kinetic energy listed in Table 2, $E_w = 7 \times 10^{49}$ erg, and taking into account that the stellar wind has blown during $t_d = 2 \times 10^6$ yr, we derive a mechanical luminosity L_w $(= E_w/t_d) = 1.2 \times 10^{36}$ erg s^{-1}, a typical value for an O-type star progenitor of the present WR star.

We note that the HI bubble could have also been created during the present WR phase of the star. An estimate of the mass loss rate of WR 53 can be obtained from radio continuum observations. WR 53 was not included in the published distance-limited sample of southern WR stars of the southern hemisphere within 3 kpc by Leitherer, Chapman, & Koribalski (1997). Observations of WR 53 were made by Thutill and colaborators with ATCA telescope (2000, ATCA website). The observations at 1384, 2496, 4800 and 8640 MHz left the star undetected within the observational limits of 0.7, 0.4, 0.2 and 0.2 mJy beam^{-1} (3 sigma), respectively (Tuthill 2007, private comunication). Assuming thermal emission, we used the expression by Wright & Barlow (1975 equation (20)), to estimate the upper limit to the mass loss rate. The values of mean molecular weight, mean number of electrons per ion, free-free Gaunt factor and rms ionic charge were obtained from Leitherer et al. (1997) for a WC8/9 star. Adopting a terminal velocity V_w=1400 km s^{-1} (Torres, Conti, & Massey 1986), a distance of 5 kpc and the radio flux limit of 0.2 mJy beam^{-1} at 8.64 GHz, we derived an upper limit for the mass loss rate $\dot{M} < 5\times10^{-5}\ M_\odot$/yr.

Adopting a conservative mass loss rate $\dot{M}=2\times10^{-5}\ M_\odot$/yr (Cappa, Goss, & van der Hucht 2004), a terminal velocity V_w=1400 km s^{-1}, and $t_d=5\times10^5$ yr (corresponding to the duration of the WR phase of a massive star), ϵ=0.01, indicating that the stellar wind energy of the WR itself would be enough to create the bubble.

The probable interstellar bubble associated with WR 53 has been detected only in the HI 21-cm line emission distribution. Other HI interstellar bubbles around WR stars were also detected only in the neutral hydrogen distribution, like the bubbles around WR 65, WR 67, WR 126, WR 154, and WR 155 (Cichowolsky & Arnal 2004; Giacani & Dubner 2004).

5. SUMMARY

The inspection of optical images at l=307° revealed the presence of an uncatalogued nebula centered at (l,b)=(307°16′, +0°16′), which was named G307.27+0.27. The optical nebula, of about 9′ radius, has a shell-like appearance. The analysis of distribution of the interstellar extinction and the IR emission suggests that the shell-like appearance is due to the presence of foreground interstellar dust.

The analysis of the HI emission distribution allowed the identification of a neutral atomic gas void and shell centered at (l,b,v)=(307°18′, +0°18′, −42 km s^{-1}), named GSH 307.3+0.3–42, of about 42 pc in size, expanding at 15 km s^{-1}. The morphological coincidence between the nebula and the HI cavity strongly suggests that both features are related.

G307.27+0.27 and its neutral atomic gas counterpart GSH 307.3+0.3–42 are located at 4 kpc in the Scuttum-Crux spiral arm.

The nebula and the HI void coincide in position with low CO and far infrared emission regions, suggesting that the molecular gas and most of the interstellar dust have been swept-up.

The nebula was not detected in the radio continuum at 5 GHz. From the rms flux density at this frequency, upper limits of $\cong$ 2 cm^{-3} and 900 $M_\odot$ were estimated for the electron density and the ionized mass.

The presence of the O6 star S 221 projected within the borders of the nebula, close to the high density section of the shell, and at a distance compatible with the one of the HI shell, supports an HII region/interstellar bubble interpretation. The UV photon flux of the O6 star and the mechanical energy of the stellar wind, derived adopting conservative stellar wind parameters, are enough to originate G307.27+0.27 and GSH 307.3+0.3–42.

We also report the discovery of a probable HI interstellar bubble associated with the Wolf-Rayet star WR 53. The structure, of 26 pc radius, was created by the WR star and its massive progenitor.

We thank R. Barbá for helpful comments on the paper and T. Dame for making his CO data available to us. We also thank P. Thutill, Q. Parker, P. Benaglia, and G. Solivella. We acknowledge the anonymous referee for valuable comments. This project was partially financed by the Consejo Nacional de Investigaciones Científicas y Técnicas (CONICET) of Argentina under project PIP 5886/05, FCAG, UNLP, under project 11/G072, and Agencia de Promoción Científica under project PICT 14018. The Digitized Sky Survey (DSS) was produced at the Space Telescope Science Institute under US Government grant NAGW-2166.

REFERENCES

Brand, J., & Blitz, L. 1993, A&A, 275, 67
Cappa, C. E., Arnal, E. M., Cichowolski, S., Goss, W. M., & Pineault, S. 2003, in IAU Symp. 212, A Massive Star Odyssey: From Main Sequence to Supernova, ed. K. van der Hucht, A. Herrero, & C. Esteban (San Francisco: ASP), 596
Cappa, C., Goss, W. M., & van der Hucht, K. A. 2004, AJ, 127, 2885
Caswell, J. L., & Haynes, R. F. 1987, A&A, 171, 261
Cesarsky, D., Lequeux, J., Abergel, A., Perault, M., Palazzi, E., Madden, S., & Tran, D. 1996, A&A, 315, 309
Cichowolski, S., & Arnal, E. M. 2004, A&A, 414, 203
Clark, J. S., & Porter, J. M. 2004, A&A, 427, 839
Condon, J. J., Griffith, M. R., & Wright, A. E. 1993, AJ, 106, 1095
Conti, P. S., & Vacca, W. D. 1990, AJ, 100, 431
Cooper, R. L., Guerrero, M. A., Chu Y.-H., Chen, C. H. R., & Dunne, B. C. 2004, ApJ, 605, 751
Dame, T. M., Hartmann, D., & Thaddeus, P. 2001, ApJ, 547, 792
Deharveng, L., Zavagno, A., Salas, L., Porras, A., Caplan, J., & Cruz-González, I. S. 2003, A&A, 399, 113
Dias, W. S., Alessi, B. S., Moitinho, A., & Lepine, J. R. D. 2002, A&A, 389, 871

Dickinson, C., Davies, R. D., & Davies, R. J. 2003, MNRAS, 341, 369
Dobashi, K., Uehara, H., Kandori, R., Sakurai, T., Kaiden, M., Umemoto, T., & Sato, F. 2005, PASJ, 57, S1
Dubner, G. 2002, in IAU Symposium 199, The Universe at Low Radio Frequencies, ed. A. Pramesh Rao, G. Swarup, & Gopal-Krishna (San Francisco: ASP), 284
Duncan, A. R., Stewart, R. T., Haynes, R. F., & Jones, K. L. 1995, MNRAS, 277, 36
Dyson, J. E. 1977, A&A, 59, 161
Georgelin, Y. M., Boulesteix, Y. P., Georgelin, Y. P., Le Coarer, E., & Marcelin, M. 1988, A&A, 205, 95
Giacani, E., & Dubner, G. 2004, A&A, 413, 225
Kuchar, T. A., & Clark, F. O. 1997, ApJ, 488, 224
Leger, A., & Puget, J. L. 1984, A&A, 137, L5
Leitherer, C., Chapman, J. M., & Koribalski, B. 1997, ApJ, 481, 898
Marston, A. P., Chu, Y.-H., & Garcia-Segura, G. 1994, ApJS, 93, 229
Martins, F., Schaerer, D., & Hillier, D. J. 2005, A&A, 436, 1049
McClure-Griffiths, N. M., Dickey, J. M., Gaensler, B. M., Green, A. J., Haverkorn, M., & Strasser, S. 2005, ApJS, 158, 178
McCray, R. 1983, Highlights Astron., 6, 565
McGruder, III, C. H. 1975, A&AS, 22, 161
Mezger, P. G., & Henderson, A. P. 1967, ApJ, 147, 471
Oster, L. 1961, Rev. Mod. Phys., 33, 525
Parker, Q. A., et al. 2005, MNRAS, 362, 689
Pierce, M. J. 2005, PhD Thesis, University of Bristol, UK
Smith, L. F., Shara, M. M., & Moffat, A. F. J. 1990, ApJ, 358, 229
Subramaniam, A., Gorti, U., Sagar, R., & Bhatt, H. C. 1995, ApJS, 302, 86
Torres, A. V., Conti, P. S., & Massey, P. 1986, ApJ, 300, 379
Vacca, W. D., Garmany, C. D., & Shull, J. M. 1996, ApJ, 460, 914
van der Hucht, K. A. 2001, NewA Rev., 45, 135
Weaver, R., McCray, R., Castor, J., Shapiro, P., & Moore, R. 1977, ApJ, 218, 377
Wright, A. E., & Barlow, M. J. 1975, MNRAS, 170, 41

M. C. Martín, C. E. Cappa, and J. C. Testori: Instituto Argentino de Radiostronomía, Parque Pereyra Iraola Km 40, Apdo. Postal 1894 (Villa Elisa), Provincia Buenos Aires, Argentina (cmartin@iar.unlp.edu.ar).